Metabolic Engineering 73 (2022) 91–103

Contents lists available at ScienceDirect

Metabolic Engineering

journal homepage: www.elsevier.com/locate/meteng

Communities of Niche-optimized Strains (CoNoS) – Design and creation of stable, genome-reduced co-cultures

Simone Schito [a,1], Rico Zuchowski [a,1], Daniel Bergen [a], Daniel Strohmeier [a], Bastian Wollenhaupt [a], Philipp Menke [a], Johannes Seiffarth [a], Katharina Nöh [a], Dietrich Kohlheyer [a], Michael Bott [a], Wolfgang Wiechert [a,b], Meike Baumgart [a], Stephan Noack [a,*]

[a] Institut für Bio- und Geowissenschaften, IBG-1: Biotechnologie, Forschungszentrum Jülich, Jülich, Germany
[b] Computational Systems Biotechnology (AVT.CSB), RWTH Aachen University, D-52074, Aachen, Germany

ARTICLE INFO

Keywords:
Microbial communities
Synthetic cocultures
C. glutamicum
Genome reduction

ABSTRACT

Current bioprocesses for production of value-added compounds are mainly based on pure cultures that are composed of rationally engineered strains of model organisms with versatile metabolic capacities. However, in the comparably well-defined environment of a bioreactor, metabolic flexibility provided by various highly abundant biosynthetic enzymes is much less required and results in suboptimal use of carbon and energy sources for compound production. In nature, non-model organisms have frequently evolved in communities where genome-reduced, auxotrophic strains cross-feed each other, suggesting that there must be a significant advantage compared to growth without cooperation. To prove this, we started to create and study synthetic communities of niche-optimized strains (CoNoS) that consists of two strains of the same species *Corynebacterium glutamicum* that are mutually dependent on one amino acid. We used both the wild-type and the genome-reduced C1* chassis for introducing selected amino acid auxotrophies, each based on complete deletion of all required biosynthetic genes. The best candidate strains were used to establish several stably growing CoNoS that were further characterized and optimized by metabolic modelling, microfluidic experiments and rational metabolic engineering to improve amino acid production and exchange. Finally, the engineered CoNoS consisting of an L-leucine and L-arginine auxotroph showed a specific growth rate equivalent to 83% of the wild type in monoculture, making it the fastest co-culture of two auxotrophic *C. glutamicum* strains to date. Overall, our results are a first promising step towards establishing improved biobased production of value-added compounds using the CoNoS approach.

1. Introduction

Current bioprocesses for the production of value-added compounds are mainly based on pure cultures that are composed of rationally engineered strains of platform organisms with versatile metabolic capacities. These strains often possess vast overcapacities of specific central metabolic proteins, a natural mechanism to cope with rapidly changing environmental conditions. On the one hand, a complex genome confers robustness to a cell, but on the other hand, it affects the predictability for biotechnological applications (Wynands et al., 2019).

In support of this, O'Brien and co-workers recently performed a genome-scale analysis of absolute protein data originating from *Escherichia coli* experiments across 16 different environments (O'Brien et al., 2016). They argue that almost half of the proteome mass is unused in certain environments and, most importantly, reduction in unused protein expression is shown to be a common mechanism to increase cellular growth rates in adaptive evolution experiments.

For another industrially important organism, *Corynebacterium glutamicum*, two quantitative proteomics studies showed that: *i)* the cellular amount of various central metabolic enzymes is much higher than necessary for maintaining optimal growth in bioreactor environments (Voges et al., 2015), and *ii)* cells maintain stable enzyme concentrations when grown on a specific primary carbon source, independent of its availability (Noack et al., 2017). This means that even under substrate

* Corresponding author. Institute of Bio- and Geosciences, IBG-1: Biotechnology, Forschungszentrum Jülich GmbH, Jülich, D-52425, Germany.
E-mail address: s.noack@fz-juelich.de (S. Noack).
[1] These authors contributed equally to this work.

https://doi.org/10.1016/j.ymben.2022.06.004
Received 1 March 2022; Received in revised form 20 May 2022; Accepted 17 June 2022
Available online 21 June 2022
1096-7176/© 2022 The Authors. Published by Elsevier Inc. on behalf of International Metabolic Engineering Society. This is an open access article under the CC BY license (http://creativecommons.org/licenses/by/4.0/).

limiting conditions, *e.g.*, in a fed-batch scenario without overfeeding, a significant amount of carbon and energy is captured in unused proteins. In other words, in the comparably well-defined environment of a bioreactor, metabolic flexibility provided by overexpression of biosynthetic genes is much less required and results in suboptimal production processes due to the waste of carbon and energy sources that could be re-directed toward a more efficient bio-production.

Synthetic genome reduction is one promising strategy to reduce these undesired protein overcapacities. Recently, we constructed a genome-reduced chassis of *C. glutamicum* by following comprehensive gene deletions including those for the three prophages, IS elements and several other genes not relevant for growth under defined D-glucose conditions (Baumgart et al., 2013, 2018; Unthan et al., 2015). The resulting strain, denoted as C1*, possesses a genome reduced by 13.4%. However, no significant increase in specific growth rate was observed compared to the wild type under various conditions.

To find an explanation for this surprising finding, we performed a comparative analysis of natural and synthetic reduced genomes and their corresponding ecological niches (Noack and Baumgart, 2019). This analysis revealed that: *i)* only deleting expressed genes can lead to noticeable carbon and energy savings that are useable for improving biomass or product synthesis; *ii)* such streamlined strains cannot exist as pure cultures but depend on the environment, *e.g.*, another community member, to complement deleted functions, and *iii)* bacterial cross-feeding interactions have evolved quite frequently in nature and, thus, there must be significant advantages for such communities.

We therefore introduced the term "Communities of Niche-optimized Strains" (CoNoS). More specifically, a CoNoS consists of at least two strains of the same species, each carrying one or more auxotrophy (Fig. 1). The strains are supposed to cross-feed each other and thereby save carbon and energy by sharing the available enzymatic capacity for the required amino acids. In this way, the strains involved in a CoNoS create a synthetic niche that mimics the naturally occurring community interactions.

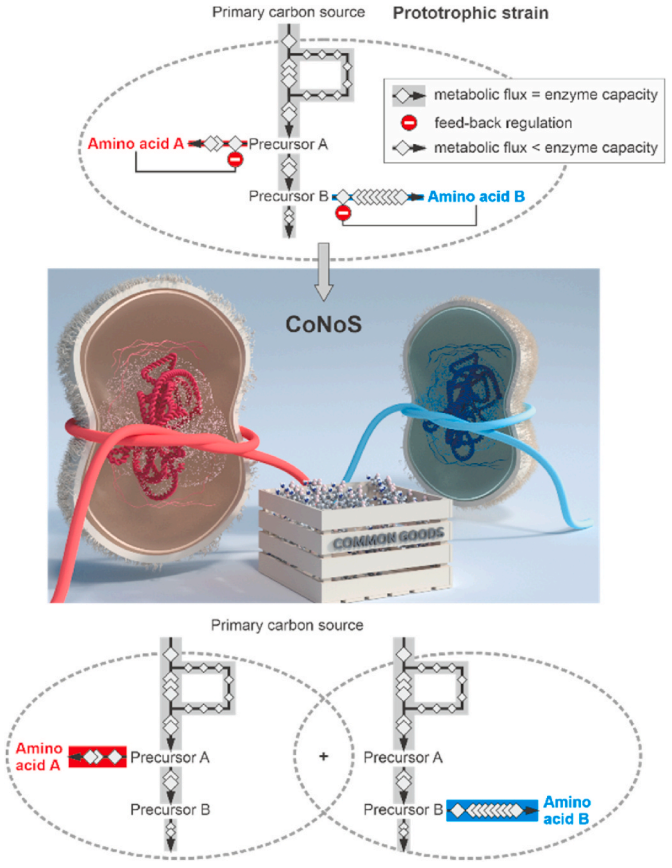

Fig. 1. CoNoS-framework for the design and creation of stable, genome-reduced co-cultures for improved amino acid production utilizing synthetic bacterial communities. As an example, the creation of a CoNoS is depicted that consists of two streamlined strains that are additionally made auxotrophic for amino acids A and B, respectively, to introduce cross-feeding interactions for these common goods.

Moreover, as McCarty and Ledesma-Amaro have pointed out, switching bioproduction from monocultures to synthetic microbial communities of auxotrophs offers many other potential advantages (McCarty and Ledesma-Amaro, 2019). One of these relates to modularity and the ability to partition engineered biosynthetic pathways among specialized strains, which could facilitate the process of metabolic engineering and reduce cross-reactivities through compartmentalization.

In this study, we successfully designed and engineered CoNoS that consists of two strains of the model organism *C. glutamicum*. We have succeeded in establishing stable, genome-reduced and fast-growing CoNoS based on greatly increased amino acid exchange rates. Based on a comprehensive characterization of engineered CoNoS, the challenges in strain and process development are discussed to establish such synthetic communities for efficient bioproduction in the near future.

2. Results

2.1. Model-based design of C. glutamicum CoNoS

For the design and stable operation of a CoNoS, the strain engineering and target product selection underlies two major criteria:

1) Introduced auxotrophies should result in a significant release of carbon and energy due to the lack of expressed genes.
2) External supply of the essential metabolite should allow full complementation of the introduced auxotrophy. This is of particular importance for the independent phenotyping of engineered strains under different environmental conditions.

Following these criteria, we decided to focus on the creation of CoNoS for the overproduction of selected proteinogenic amino acids.

We started with an *in silico* feasibility analysis for introducing single amino acid auxotrophies in *C. glutamicum*. Briefly, by taking all 20 proteinogenic amino acids into account, we performed constraint-based flux balance analysis (cFBA) using an extended genome-scale model and a newly created focused network model of *C. glutamicum*. Auxotrophies were modeled by blocking at least one essential reaction step in the corresponding amino acid biosynthetic pathway at a time. Optimal cell growth was simulated with D-glucose as primary carbon and energy source and by allowing unrestricted uptake of the essential amino acid (for details see Material and Methods section).

As a result, most amino acid auxotrophic strains under supplemented conditions are theoretically feasible and the simulated growth phenotypes are consistent with our CoNoS approach (Fig. 2A). As expected, the predicted optimal growth rates were always higher than for the wild type, because more carbon is supplied via the corresponding essential amino acid in addition to a fixed amount of D-glucose (Fig. 2B). Depending on the individual demand of the amino acid for biomass generation and its position in the metabolic network, this growth rate effect might be comparably low (<1% for L-tryptophan, L-histidine and L-cysteine) or high (>10% for L-aspartate and L-asparagine). It is important to note that due to a lack of empirical data, both models do not account for a potential growth advantage of auxotrophic strains in terms of lower gene expression and lower protein production costs (see criterion 1), and the predicted increases in growth rate should not be misinterpreted in this regard.

Exceptions were found for L-glutamate and L-glutamine, whose simulated auxotrophies led to unreasonably high growth rates. Both

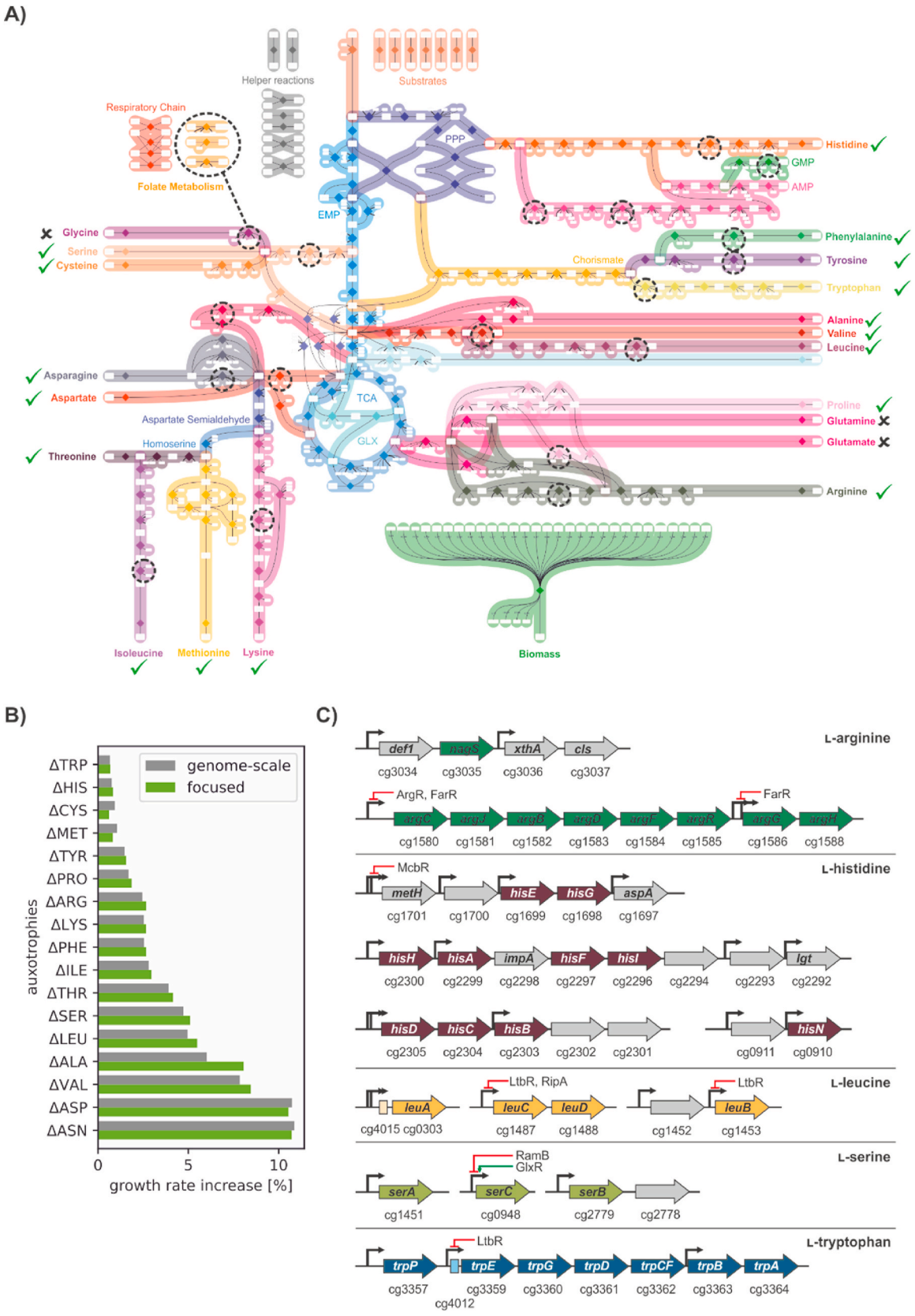

Fig. 2. Model-based design of *C. glutamicum* CoNoS. A) Focused metabolic network model of *C. glutamicum*. Feasible amino acid auxotrophies are check-marked in green. Non-feasible auxotrophies are cross-marked in black and corresponding linkages to the C1 metabolism (L-glycine) as well as transaminase reactions (L-glutamate and L-glutamine) are additionally highlighted. B) Predicted increases in growth rate when single amino acid auxotrophic strains are cultured under supplemented conditions. C) Structural genes encoding the enzymes for synthesis of those amino acids selected for introducing auxotrophies.

amino acids play essential roles in the transamination of different metabolic compounds such as the 2-oxo precursors of most proteinogenic L-amino acids in *C. glutamicum* (Eggeling and Bott, 2005). These transaminations lead either to the formation of additional L-glutamate (in the case of L-glutamine as amine source) or directly to α-ketoglutarate, which can be recycled in the tricarboxylic acid cycle (cf. Fig. 2A). Conclusively, strain designs carrying single amino acid auxotrophies for L-glutamate and L-glutamine are not sufficiently defined for our modelling-assisted CoNoS approach (see criterion 2).

Furthermore, simulation of an L-glycine-auxotrophic strain is not feasible because the required inactivation of the L-serine hydroxyl methyltransferase step (encoded by *glyA*) then also prevents recycling of tetrahydrofolate into 5,10-methylene-tetrahydrofolate. The latter is the major source of C1 units in the cell, making GlyA a key enzyme in the biosynthesis of purines, thymidine, methionine, choline and lipids. In fact, the gene *glyA* is essential in *C. glutamicum* (Peters-Wendisch et al., 2005), but it can be deleted in *E. coli* (Mundhada et al., 2016; Vidal et al., 2008).

Following the *in silico* analysis, we thoroughly studied the transcriptional and metabolic organization of all encoding genes and catalytic enzymes for the synthesis of the 17 proteinogenic amino acids in *C. glutamicum*. We utilized our revised genome annotation list (Baumgart et al., 2018) and the following criteria:

1) Target genes should be organized in one or only a few transcriptional units to allow easy and full deletion of the pathway.
2) Deletion of target genes does not affect transcription of neighboring genes.
3) Associated operons do not contain any relevant genes not related to the amino acid synthesis pathway.

The data obtained were compared with the known demand of each amino acid for biomass synthesis in order to evaluate the potential of a corresponding auxotrophic strain in a CoNoS setting. Finally, our evaluation resulted in the selection of the five amino acids L-arginine, L-histidine, L-leucine, L-serine, and L-tryptophan for establishing CoNoS for amino acid overproduction (Fig. 2C).

2.2. Construction and phenotyping of selected auxotrophic strains

Amino acid auxotrophic strains were constructed by deleting the whole biosynthetic machinery for the respective amino acids L-arginine, L-histidine, L-leucine, L-serine or L-tryptophan (Fig. 2C). Both *C. glutamicum* ATCC 13032 (WT) and the derived genome-reduced *C. glutamicum* C1* (Baumgart et al., 2018) were used as precursor strain. The deletion of the L-histidine biosynthetic machinery is not possible in the C1* background because of the missing L-histidine importer PheP (cg1305) as shown previously (Kulis-Horn et al., 2014). In total, nine auxotrophic strains were constructed that are listed in Table 1. The auxotrophy of each newly constructed strain will be indicated with the Δ symbol followed by the amino acid abbreviation, *e.g.*, ΔARG has the whole L-arginine biosynthetic machinery deleted.

Subsequently, the growth performance of all engineered strains was tested by running small-scale cultures in a BioLector system. Defined CGXII medium with D-glucose as primary carbon and energy source was applied and the corresponding amino acid was supplemented at different concentrations (Fig. 3A). All auxotrophic strains were not able to grow under non-supplemented conditions, confirming the success of the prior genome reduction step. Furthermore, the minimal amount of amino acid supplementation to reach growth at wild-type levels was identified for the L-arginine, L-leucine, and L-serine auxotrophic strains. Interestingly, none of these strains showed a higher growth rate as was predicted by the *in silico* analyses (cf. Fig. 2B). In particular, for the L-leucine and L-serine strains, a 5% increase from 0.59 ± 0.01 h^{-1} (measured control) to 0.62 h^{-1} (simulated auxotrophy) could have been detected, taking into account the measurement accuracy. This is

Table 1
Bacterial strains used in this study.

Strain	Characteristics	Reference
E. coli		
DH5α	F-Φ80*dlac*Δ(*lacZ*)M15 Δ(*lacZYA-argF*) U169 *endA1 recA1 hsdR17* (rK- mK+) *deoR thi-1 phoA supE44 λ- gyrA96 relA1*; strain used for cloning procedures	Hanahan (1983)
C. glutamicum		
ATCC 13032 (WT)	Biotin-auxotrophic wild type	Kinoshita et al. (1957)
C1*	Derivative of ATCC 13032 with a genome reduced by 13.4%	Baumgart et al. (2018)
C1* ΔTRP	C1* with an in-frame deletion of Δ*trpP* (cg3357) Δ*trpE* (cg3359) Δ*trpG* (cg3360) Δ*trpD* (cg3361) Δ*trpCF* (cg3362) Δ*trpB* (cg3363) Δ*trpA* (cg3364)	This study
WT* ΔTRP	WT with an in-frame deletion of Δ*trpP* (cg3357) Δ*trpE* (cg3359) Δ*trpG* (cg3360) Δ*trpD* (cg3361) Δ*trpCF* (cg3362) Δ*trpB* (cg3363) Δ*trpA* (cg3364)	This study
C1* ΔSerA	C1* with an in-frame deletion of Δ*serA* (cg1451)	This study
C1* ΔSerAC	C1* ΔSerA with an in-frame deletion of Δ*serC* (cg0948)	This study
C1* ΔSER	C1* ΔSerAC with an in-frame deletion of Δ*serB* (cg2779)	This study
WT ΔSerA	WT with an in-frame deletion of Δ*serA* (cg1451)	This study
WT ΔSerAC	WT ΔSerA with an in-frame deletion of Δ*serC* (cg0948)	This study
WT ΔSER	WT ΔSerAC with an in-frame deletion of Δ*serB* (cg2779)	This study
C1* ΔLeuA	C1* with an in-frame deletion of Δ*leuA* (cg0303)	This study
C1* ΔLeuACD	C1* ΔLeuA with an in-frame deletion of Δ*leuC* (cg1487) Δ*leuD* (cg1488)	This study
C1* ΔLEU	C1* ΔLeuACD with an in-frame deletion of Δ*leuB* (cg1453)	This study
WT ΔLeuA	WT with an in-frame deletion of Δ*leuA* (cg0303)	This study
WT ΔLeuACD	WT ΔLeuA with an in-frame deletion of Δ*leuC* (cg1487) Δ*leuD* (cg1488)	This study
WT ΔLEU	WT ΔLeuACD with an in-frame deletion of Δ*leuB* (cg1453)	This study
C1* ΔNagS	C1* with an in-frame deletion of Δ*nagS* (cg3035)	
C1* ΔARG	C1* ΔNagS with an in-frame deletion of Δ*argC* (cg1580) Δ*argJ* (cg1581) Δ*argB* (cg1582) Δ*argD* (cg1583) Δ*argF* (cg1584) Δ*argR* (cg1585) Δ*argG* (cg1586) Δ*argH* (cg1588)	This study
WT ΔNagS	WT with an in-frame deletion of Δ*nagS* (cg3035)	
WT ΔARG	WT ΔNagS with an in-frame deletion of Δ*argC* (cg1580) Δ*argJ* (cg1581) Δ*argB* (cg1582) Δ*argD* (cg1583) Δ*argF* (cg1584) Δ*argR* (cg1585) Δ*argG* (cg1586) Δ*argH* (cg1588)	This study
WT ΔHisEG	WT with an in-frame deletion of Δ*hisE* (cg1699) Δ*hisG* (cg1698)	This study
WT ΔHisEGHAF	WT ΔHisEG with an in-frame deletion of Δ*hisH* (cg2300) Δ*hisA* (cg2299) Δ*impA* (cg2298) Δ*hisF* (cg2297) Δ*hisI* (cg2296)	This study
WT ΔHisEGHAFDCB	WT ΔHisEGHAF with an in-frame deletion of Δ*hisD* (cg2305) Δ*hisC* (cg2304) Δ*hisB* (cg2303)	This study
WT ΔHIS	WT ΔHisEGHAFDCB with an in-frame deletion of Δ*hisN* (cg0910)	This study
C1* ΔARG LEU$^+$	C1* ΔARG with an exchange of *leuA* (cg0303) 180 bp upstream region including the leader peptide and native promoter with *tuf* promoter	This study
C1* ΔLEU ARG$^+$	C1* ΔLEU with in frame-deletion of Δ*argR* (cg1585)	This study
C1* ΔTRP LEU$^+$	C1* ΔTRP with an exchange of *leuA* (cg0303) 180 bp upstream region	This study

(*continued on next page*)

Table 1 (*continued*)

Strain	Characteristics	Reference
	including the leader peptide and native promoter with *tuf* promoter	
C1* ΔLEU TRP^{+}	C1* ΔLEU with point mutations *trpL*$_{fbr}$ TrpE$_{S38R}$ (Cg3359)	This study
WT ΔHIS TRP^{+}	WT ΔHIS with point mutations *trpL*$_{fbr}$ TrpE$_{S38R}$ (Cg3359)	This study
WT ΔTRP HIS^{+}	WT ΔTRP with point mutation HisG$_{A270D}$ (Cg1698)	This study
WT ΔARG LEU^{++}	WT ΔARG with exchange of *leuA* (cg0303) and 180 bp upstream region to *leuA*_B018 (B018: L-leucine producing *C. glutamicum* strain created by random mutagenesis) under control of the *tuf* promoter	This study
C1* ΔLEU ARG^{++}	C1* ΔLEU ARG^{+} with point mutations ArgB$_{A26V\ M31V}$ (Cg1582)	This study
C1* ΔLEU ARG^{+}:: P$_{tac}$-eYFP	C1* ΔLEU ARG^{+} with eYFP fluorescent protein under control of tac promoter integrated in the IGR between cg1121 and cg1122	This study
WT ΔLEU ARG^{++}:: P$_{tac}$-eYFP	WT ΔLEU ARG^{+} with eYFP fluorescent protein under control of tac promoter integrated in the IGR between cg1121 and cg1122	This study
WT ΔARG LEU^{++}:: P$_{tac}$-crimson	WT ΔARG LEU^{++} with crimson fluorescent protein under control of tac promoter integrated in the IGR between cg1121 and cg1122	This study

surprising since we also expected an additional growth advantage of these auxotrophs through the deletion of the strongly expressed amino acid biosynthetic genes.

In case of the L-histidine and L-tryptophan auxotrophs, the specific growth rate was strongly reduced compared to the wild type (Fig. 3A). This effect could be due to several reasons and one can speculate about a general limitation of the uptake of the corresponding amino acid, a down-regulation of the D-glucose uptake or an accumulation of growth-inhibitory intermediates as a consequence of enzyme inactivation and the lack of complete biosynthetic pathways. Clearly, a slow-growing auxotrophic strain is less suitable for a CoNoS because it would affect the performance of the entire co-culture due to the mutual exchange of amino acids required for growth. Except for the L-tryptophan auxotrophic strain, no difference in growth rates were detected between the strains based on the C1* and wild type, respectively (data not shown).

2.3. Setup and engineering of stable CoNoS

With the strains auxotrophic for 5 different amino acid at hand, we could potentially establish 10 different CoNoS. To pre-select pairs of interest, we performed *in silico* co-culture simulations using a similar model-based design as for the single cFBA, but now applying the SteadyCom approach (for details see Material and Methods section).

In general, the predicted relative abundances in the simulated co-cultures are consistent with the results of the cFBA approach. Auxotrophic strains exhibiting a higher increased growth rate under supplemented conditions also occurred in lower fractions in the corresponding CoNoS setting (cmp. Figs. 2B and 3B). These uneven distributions are

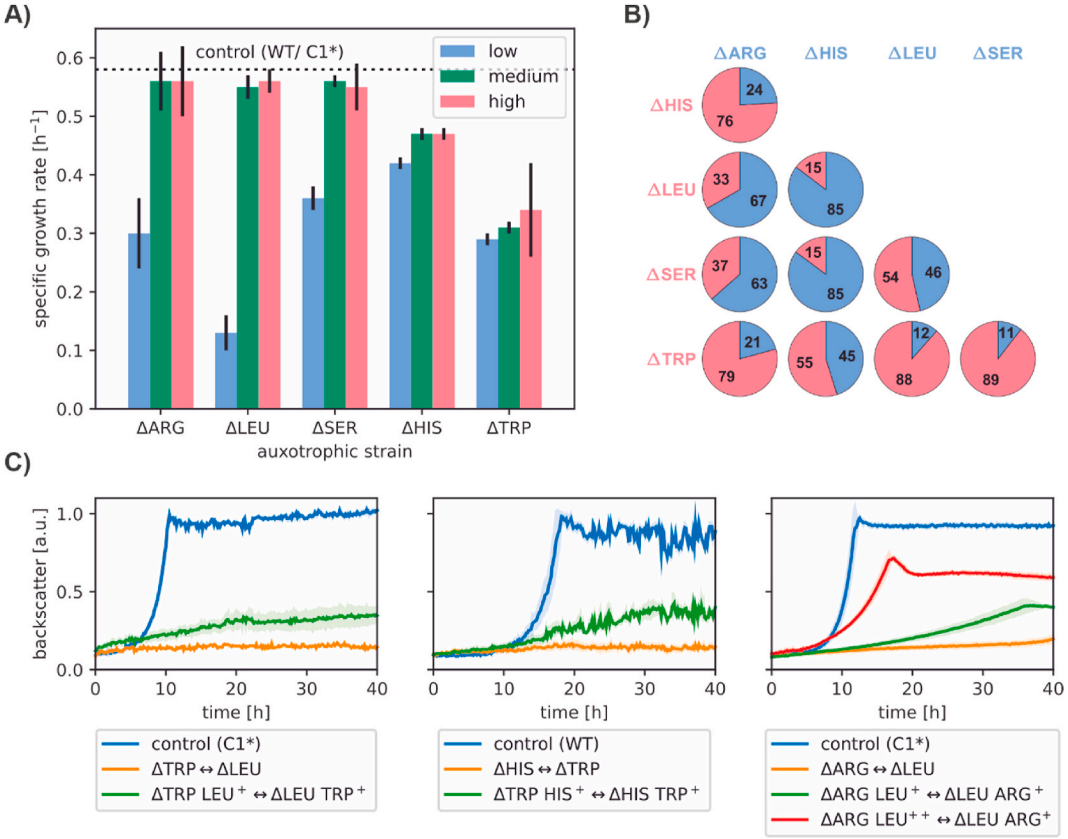

Fig. 3. Setup of stable CoNoS. A) Growth performance of engineered auxotrophic strains. Cultures were performed in triplicate in defined CGXII medium containing 111 mM D-glucose and different additions of the corresponding amino acid. B) *In silico* prediction of relative abundances of selected auxotrophic strains in different co-culture combinations. C) Growth performance of selected CoNoS. Cultures were performed in triplicate in non-supplemented CGXII medium with 111 mM D-glucose. Further engineered strains are marked with a plus sign. The predecessor used for the correspondent strain construction (*C. glutamicum* C1* or WT) was cultivated as a positive control. Backscatter data were normalized by the maximum value recorded for each positive control culture. Mean values and standard deviations are shown as lines and shaded areas, respectively.

due to different demands of the amino acids for the cellular composition of *C. glutamicum*. For example, the demand of L-histidine for protein synthesis (0.066 mmol g^{-1}) is nearly two thirds lower as compared to L-arginine (0.188 mmol g^{-1}), which explains the predicted ratio of 76:24.

From these results we selected three pairs of auxotrophs whose predicted distributions span a certain range and whose introduced auxotrophies partially overlap, namely ΔTRP ↔ ΔLEU, ΔHIS ↔ ΔTRP and ΔARG ↔ ΔLEU. All three CoNoS were cultivated under non-supplemented D-glucose conditions in a BioLector. Low cell population growth was observed only for the CoNoS consisting of the L-arginine and L-leucine-auxotrophic strains (Fig. 3C). The two strains, although highly inefficient, were able to mutually exchange the required amount of amino acids to establish a growing co-culture. Using an endpoint sample and considering 47 clones, we analyzed the ratio of the two strains by colony PCR. This resulted in a distribution of 83:17 for the ΔARG and ΔLEU strains, respectively. This ratio is significantly higher as compared to the model predictions (67:33, cf. Fig. 3B) and indicates an unbalanced amino acid exchange between the two CoNoS partners with L-leucine as the limiting factor.

To establish more balanced co-cultures, we further engineered all strains toward higher production of the corresponding cross-fed amino acid. To this end, reversal of feedback inhibition in the selected auxotrophs is a straightforward approach with minimal metabolic engineering. For enhancing L-arginine biosynthesis, relieving the feedback inhibition of the *arg*-operon can be realized by deleting its repressor, namely *argR* (cf. Fig. 2C) (Ikeda et al., 2009). In case of L-histidine, the feedback inhibition can be interrupted by introducing a mutation in HisG (A270D) (Kulis-Horn et al., 2015). The regulation of L-tryptophan can be circumvented by mutating the attenuator *trpL* as well as TrpE (S38A) (Matsui et al., 1987). Finally, in L-leucine biosynthesis, the first enzyme, LeuA, is regulated via feedback inhibition. To increase L-leucine biosynthesis, the native *leuA* gene promoter and the leader peptide *leuL* were replaced by the strong promoter of the elongation factor TU (P_{tuf}) as described previously (Vogt et al., 2014).

In the following, the further engineered auxotrophic strains are labeled with the abbreviation of the target product and a plus sign indicating the level of engineering, *e.g.*, ΔARG LEU^{+} is a first generation L-leucine overproducing strain. These strains were cultivated under equal co-culture conditions as before. In all cases, CoNoS composed of strains optimized for amino acid over production resulted in stably growing co-cultures, confirming the success of the metabolic engineering strategy (Fig. 3C). Nevertheless, all co-cultures grew much slower than the corresponding control strain, still indicating a severe limitation of amino acid exchange.

2.4. Detailed phenotyping and optimization of selected CoNoS

In the following we focused on the further optimization of the ΔARG LEU^{+} ↔ ΔLEU ARG^{+} CoNoS. From the ratio estimation of the non-engineered CoNoS we found a primary bottleneck in the performance of the L-leucine producing strain. Assuming that this bottleneck is still not resolved, we further constructed the ΔARG LEU^{++} strain by exchanging the entire native *leuA* gene with the BS018 $leuA^{fbr}$ gene sequence, also under control of a P_{tuf} promotor (Vogt et al., 2014). The resulting ΔARG LEU^{++} ↔ ΔLEU ARG^{+} CoNoS showed greatly improved growth performance, reaching 75% of the final biomass of the mono-culture with the C1* control strain. The specific growth rate of 0.22 ± 0.01 h^{-1} was also significantly improved and now resembled almost 50% of wild-type level (Fig. 3C).

To study the growth behaviour of both engineered auxotrophs in the co-culture in more detail we performed cultivations in a polydimethylsiloxane (PDMS) based microfluidic cultivation device. To enable a direct visual and quantitative discrimination, the two strains ΔARG LEU^{++} and ΔLEU ARG^{+} were further engineered by integrating the fluorescent proteins crimson or eYFP, respectively, under control of the P_{tac} promoter. Protein expression was induced by the addition of 100 μM of IPTG and did not effect strain growth as shown previously (Baumgart et al., 2013). The growth behaviour of the CoNoS was observed at single cell level over a time period of 46 h (Fig. 4A and Fig. S1). Starting from a nearly balanced inoculation ratio between both CoNoS partners, the ΔARG LEU^{++} strain grew much faster within the first 10 h of cultivation. A maximum ratio of 64:36 was obtained between the ΔARG LEU^{++} and the ΔLEU ARG^{+} strain, which is close to the optimal ratio predicted by the modeling (67:33, cf. Fig. 3B). Thereafter, the availability of L-arginine became limiting and cell division slowed significantly. After 20 h of cultivation a stable growth of the CoNoS was observed, resulting in a constant distribution of 47:53 between the ΔARG LEU^{++} and the ΔLEU ARG^{+} strain (Fig. 4A). This ratio is now significantly lower as compared to the model predictions, indicating an unbalanced amino acid exchange between the two CoNoS partners with L-arginine as the limiting factor.

Closer inspection revealed that in certain areas of the microfluidic chamber where one member of the community was not near its partner, growth occurred only at the beginning of cultivation, where the cells likely relied on the remaining amino acid stores (Fig. S1A). In contrast, growth was more pronounced in areas where the two members of the community were close together. Such 'island effect', with non-growing isolated community member, was not observed in the control monoculture with the WT (Fig. S1B). This finding again supports the hypothesis that amino acid exchange is a major bottleneck of CoNoS, especially at the earliest stage of cultivation when a small number of cells are struggling to increase the concentration of amino acids.

To verify the potential limitation of L-arginine, we performed transient sampling experiments with the ΔLEU ARG^{+} and the ΔARG LEU^{++} strains, each cultivated as a monoculture in CGXII medium supplemented with 3 mM of either L-leucine or L-arginine. Only the ΔARG LEU^{++} strain showed growth-associated accumulation of L-leucine, clearly indicating a shift toward L-arginine as the limiting amino acid in the specific CoNoS (Fig. 4B).

To resolve the bottleneck in L-arginine supply, we performed additional metabolic engineering by relieving the feedback-inhibition of ArgB via the mutations A26V M31V (cf. Fig. 2C) (Ikeda et al., 2009) resulting in the ΔLEU ARG^{++} strain. Co-cultivation of the doubly engineered auxotrophs still showed a slightly delayed onset of cell population growth, but a further increased final biomass to about 86% of the control strain (Fig. 5A). Moreover, the ΔARG LEU^{++} ↔ ΔLEU ARG^{++} CoNoS showed a highly increased specific growth rate of 0.47 ± 0.01 h^{-1}, which is equivalent to 83% of the wild type. The latter points to a further increased and much more balanced amino acid exchange between the two auxotrophic strains.

However, in a co-culture such as our CoNoS, direct experimental prove is not possible because only the net accumulation of a particular amino acid species can be measured. Therefore, we followed an indirect approach by process modelling employing a segregated, unstructured model approach (Fig. 5B). In short, the model takes explicit account of the (re)action of the CoNoS with its environment via the exchange of amino acids between the two community members. Model formulation and validation was performed in a stepwise manner to allow integration of available experimental data, and to reduce the degree of freedom of unknown parameters in the final CoNoS model.

As a result, the model enables simulation of the individual growth dynamics of both CoNoS members. According to these predictions, the ΔLEU ARG^{++} strain grew a bit faster and to a slightly higher biomass, which would resemble the second growth phase during the microfluidic cultivations (cmp. Figs. 4A and 5A). Furthermore, the predicted maximum ratio of approx. 45:55 between the ΔARG LEU^{++} and the ΔLEU ARG^{++} strain is nearly identical under both conditions. Most importantly, the estimated specific rates underscore the successful engineering of this CoNoS toward higher L-arginine production performance, and the potential switch back to L-leucine as the limiting amino acid (Table 2).

To verify the predicted limitation of L-leucine and accumulation of L-

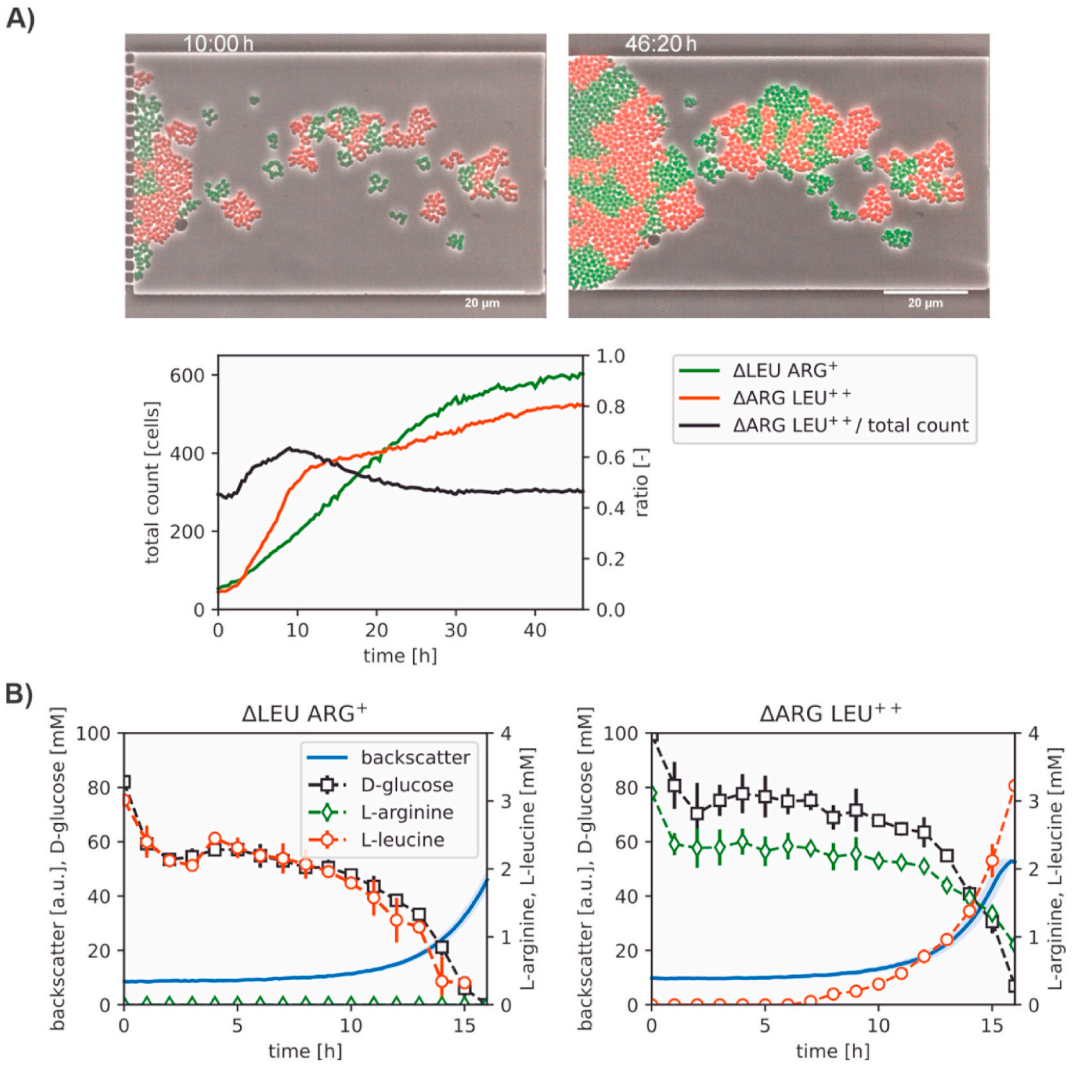

Fig. 4. Detailed phenotyping of selected CoNoS. A) Microfluidic batch cultivation of the ΔARG LEU^{++} (red) ↔ ΔLEU ARG^{+} (green) CoNoS to study co-culture dynamics at single-cell level. Cell count and resulting ratio of the two species as determined by semi-automated image analysis. B) Transient sampling experiments with engineered auxotrophic strains ΔLEU ARG^{+} and ΔARG LEU^{++}. Cultures were performed in triplicate in CGXII medium supplemented with 3 mM of either L-leucine or L-arginine.

arginine, we performed another transient sampling experiment with the best CoNoS (Fig. 6A). Indeed, only enrichment of L-arginine up to 1 mM was found, supporting the expected higher proportion of ΔLEU ARG^{++} cells in the co-culture. From the microfluidic experiments, we hypothesized that initial cell density may be a critical factor in ensuring sufficient amino acid concentration for immediate balanced co-culture growth. Indeed, a fivefold increase in initial biomass resulted in a much faster onset of exponential growth and a further increase in the maximum specific growth rate of CoNoS, which is now even close to that of the wild type (Fig. 6B).

Finally, to test the stability of the CoNoS for long-term cultures we performed a repetitive batch experiments covering ten consecutive batches (Fig. 6C). Application of the fluorescently labeled strains variants allowed online monitoring of the two CoNoS members and showed very stable dynamics of the co-culture composition along the batch series.

3. Discussion

It is widely accepted that cooperation between microorganisms plays a crucial role in the evolution of species and represents a net advantage in terms of efficiency in using the available resources (D'Souza et al., 2014). Furthermore, evolution drives genome reduction to adapt microorganisms to specific ecological niches when the supply of function occurs by a partner organism (Noack and Baumgart, 2019). Now, is it possible to re-create genome-reduced communities that exploit the available resources in a more efficient way? And, most importantly, could these synthetic communities re-direct their carbon and energy toward a more efficient bio-production? Heterogeneous microbial communities, both natural and engineered, potentially manifest higher fitness and productivity opening future perspective for synthetic novel communities that exploit cross-feeding interactions to achieve complex and/or energetically difficult tasks in a stable, robust way (Yang et al., 2020).

In the present work, we succeeded in establishing stable, genome-reduced co-cultures of *C. glutamicum* by generating single community strains carrying broad gene deletions in selected amino acid biosynthesis pathways. Most surprisingly, no fitness advantage was observed when the amino acid auxotrophic strains were cultivated in a mono-culture in supplemented media. Specific growth rate and final biomass yield were carefully analyzed in comparison with the parental non-auxotrophic strain using well-controlled microbioreactor experiments with online monitoring of biomass growth. In another study it was shown, by counting the colony-forming units after 24 h cultivation, that *E. coli*

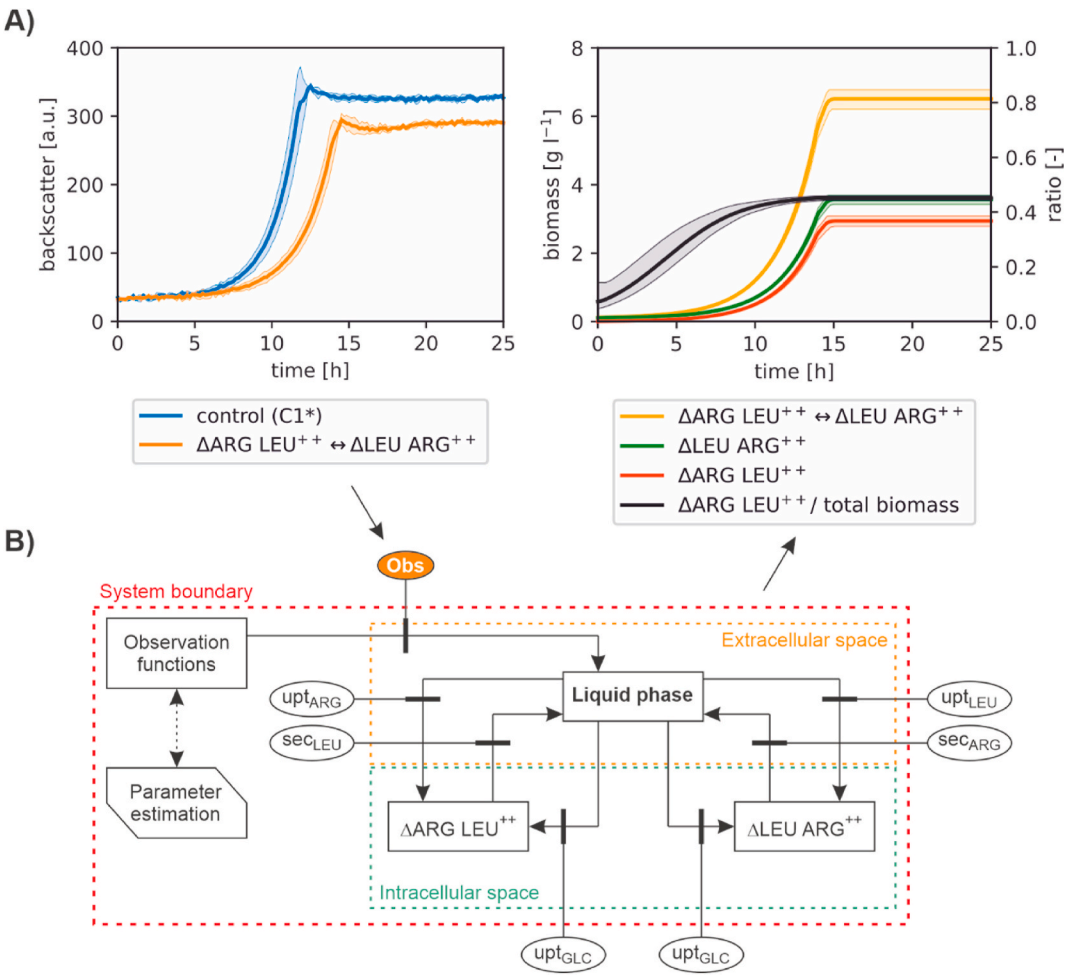

Fig. 5. Optimization and model-based analysis of selected CoNoS. A) Growth performance of multiple engineered ΔARG LEU^{++} ↔ ΔLEU ARG^{++} CoNoS. Cultures were performed in triplicate in non-supplemented CGXII medium with 111 mM D-glucose. B) Segregated, unstructured process modelling to simulate CoNoS dynamics. Based on a pre-parameterization approach, only the backscatter measurements were used as observables for final model validation and prediction of individual species growth dynamics. The confidence bounds for the state variables shown were generated by propagating the error bounds for estimated model parameters.

strains auxotrophic for different amino acids or vitamins, constructed with single-gene deletions, obtained a growth advantage of 13% compared to their parental strain (D'Souza et al., 2014). Instead, in this work, despite the growth rate increase predicted by our model-based analysis, no improved growth performances were detected, possibly due to other limitations occurring such as nutrient uptake or oxygen transfer.

In particular, the ΔHIS and ΔTRP strains not only did not reach the predicted growth benefits (Fig. 2B), but also performed worse than the WT. This indicates effects not taken into account by the model, which could be related to the uptake of the respective amino acid or yet unknown systemic effects of the deleted genes (i.e. *hisE hisG hisH hisA impA hisF hisI hisD hisC hisB* and *hisN* for the ΔHIS strain as well as *trpP trpE trpG trpD trpCF trpB* and *trpA* for the ΔTRP strain). Specifically, the uptake of L-histidine occurs in *C. glutamicum* via the transporter PheP (cg1305) and should not be impaired in the ΔHIS strain. Kulis-Horn and coworkers reported on the growth effect of single deletions of L-histidine biosynthesis genes and no other auxotrophies besides L-histidine are currently known (Kulis-Horn et al., 2014). Also, it was previously speculated about a possible role of HisA in L-tryptophan biosynthesis because in other actinobacteria missing TrpF (i.e. the HisA homologue), HisA plays a bifunctional role in both L-tryptophan and L-histidine biosynthesis (Barona-Gómez and Hodgson, 2003). In our case, however, no L-tryptophan auxotrophy occurred after the deletion of *hisA*. Moreover, L-histidine biosynthesis is linked to the *de novo* purine biosynthetic pathway via the AICAR (5′-phosphoribosyl-4-carboxamide-5-aminoimidazole) cycle, with AICAR being a byproduct of the reaction by HisFH (Alifano et al., 1996). Therefore, deletion of *hisF* and *hisH* and the resulting absence of this AICAR source might impair the *de novo* biosynthesis of AMP (adenosine monophosphate) and GMP (guanosine monophosphate). Nevertheless, the primary precursor PRPP (5-phosphoribosyl 1-pyrophosphate) of the purine pathway can still be synthesized in the ΔHIS strain, so the reasons for the slow growth rate under supplemented conditions remain elusive.

As for the other slow-growing ΔTRP strain, the uptake of L-tryptophan occurs mainly via the general amino acid importer AroP, but is has been hypothesized that there is another import system (Wehrmann et al., 1995). In particular, the *trpP* gene (cg3357) has been suggested to encode an L-tryptophan permease in *C. glutamicum* (Heery et al., 1994), and it was also accordingly annotated after genome sequencing (Kalinowski et al., 2003). Of all the tryptophan operon genes, it is also the only one that can be deleted without causing L-tryptophan auxotrophy (Mormann et al., 2006). Indeed, an L-tryptophan auxotrophic strain still possessing the *trpP* gene grew with a growth rate similar to WT (unpublished data), strongly hinting at a important role of TrpP as a permease for L-tryptophan uptake. Despite the growth limitations of the ΔHIS and ΔTRP strains, we continued to use them for setting up our synthetic communities.

Table 2
Specific uptake and production rates of engineered *C. glutamicum* amino acid producer strains during cultivation in supplemented monocultures and co-cultures, respectively. Rates were derived from model-based analysis by fitting suitable bioprocess models to the time-dependent measurements of replicate cultures in small-scale phenotyping experiments. Asymmetric confidence bounds were estimated by following a parametric bootstrapping approach.

Strain/condition	Monoculture[a]		Coculture[b]		
	ΔARG LEU^{++}	ΔLEU ARG^{+}	ΔARG LEU^{++}	ΔLEU ARG^{++}	ΔARG LEU^{++} ↔ ΔLEU ARG^{++}
Growth rate [h^{-1}]	0.41 [0.405, 0.411]	0.40 [0.397, 0.409]	0.41 [0.410, 0.411]	0.45 [0.437, 0.472]	0.44[c] [0.426, 0.444]
D-glucose uptake rate [mmol g_{CDW}^{-1} h^{-1}]	4.46 [4.428, 4.499]	5.54 [5.321, 5.903]	4.44 [4.441, 4.441]	5.52 [5.521, 5.521]	–
L-leucine uptake rate [mmol g_{CDW}^{-1} h^{-1}]	–	0.32 [0.300, 0.333]	–	0.13 [0.128, 0.138]	–
L-arginine uptake rate [mmol g_{CDW}^{-1} h^{-1}]	0.09 [0.088, 0.102]	–	0.09 [0.093, 0.093]	–	–
L-leucine production rate [mmol g_{CDW}^{-1} h^{-1}]	0.22 [0.210, 0.232]	–	0.17 [0.164, 0.173]	–	0[d] [0, 0]
L-arginine production rate [mmol g_{CDW}^{-1} h^{-1}]	–	0 [0, 0]	–	0.52 [0.305, 0.746]	0.25[e] [0.132, 0.368]

[a] Rates were constant throughout the exponential growth phase, and values represent the mean of maxima across all replicates and time points.
[b] Rates were not constant, and values represent the mean across all replicates at time $t = 12$ h (see Jupyter notebooks for details).
[c] Calculated as: $\mu_{tot} = (\mu_{\Delta ARG} \cdot X_{\Delta ARG} + \mu_{\Delta LEU} \cdot X_{\Delta LEU})/X_{tot}$
[d] Net rate calculated as: $v_{net,LEU} = (v_{syn,\ LEU,\ \Delta ARG} \cdot X_{\Delta ARG} - v_{upt,\ LEU,\ \Delta LEU} \cdot X_{\Delta LEU})/X_{tot}$
[e] Net rate calculated as: $v_{net,ARG} = (v_{syn,\ ARG,\ \Delta LEU} \cdot X_{\Delta LEU} - v_{upt,ARG,\ \Delta ARG} \cdot X_{\Delta ARG})/X_{tot}$

At this point, we established different CoNoS, each combining two different amino acid auxotrophic strains. For all CoNoS tested, growth was observed only in the ΔARG ↔ ΔLEU community. The sufficient biosynthesis and extracellular exchange of the dependent amino acids L-arginine and L-leucine allowed this CoNoS to form a niche that could support the growth of both strains. Noteworthy, it has already been shown that *C. glutamicum* (among other prokaryotic and eukaryotic model organisms) excretes amino acids such as L-arginine as a result of extended overflow metabolism (Paczia et al., 2012). Our results demonstrate that cooperation of *C. glutamicum* strains can indeed arise solely from genome reduction without further engineering, underlining the enormous potential of niche construction through bacterial cross-feeding even in a homogeneous environment (San Roman and Wagner, 2018).

However, we found that amino acid exchange was limiting for the growth of our communities and therefore proceeded with rational metabolic engineering. To strengthen cross-feeding interactions and allow overproduction of amino acids, we first relieved the corresponding end-product feed-back inhibitions, a strategy that has recently been successful in amino acid auxotrophic *E. coli* (Pande et al., 2014) and *S. cerevisiae* (Shou et al., 2007).

This indeed led to a significant increase in growth in all engineered CoNoS (Fig. 3C). However, the growth rates of the co-cultures were still below the level of the wild-type mono-culture. Therefore, we focused on the ΔARG ↔ ΔLEU CoNoS and performed further rational metabolic engineering to gradually and reciprocally debottleneck the amino acid exchange. As expected, the growth limiting bottleneck oscillated from one of the two amino acids to the other at each engineering step. This clearly shows the difficulty of optimally balancing amino acid exchange between two auxotrophic strains in a purely rational manner.

Nevertheless, the final engineered CoNoS ΔARG LEU^{++} ↔ ΔLEU ARG^{++} showed a specific growth rate and biomass titer of approximately 83% and 86% of the control strain, respectively (Fig. 5A). Because the applied metabolic engineering steps in ΔARG LEU^{++} and ΔLEU ARG^{++} were already sufficient to achieve nearly optimal cross-feeding interactions, it is unclear whether a further increase in amino acid production can improve the growth of CoNoS. Nevertheless, further improvements are desirable, since a slightly delayed onset of exponential growth and lower biomass formation occurred in the co-culture, while neither effect occurred in the supplemented monocultures.

At this point, the L-leucine production could be further increased by integrating more copies of the gene encoding the feedback-resistant LeuA into the ΔARG LEU^{++} strain, by deleting *ltbR*, encoding the repressor of *leuBCD*, by increasing D-glucose uptake or by increasing precursor supply as achieved in the currently best L-leucine producer strain MV-Leu F2 (Vogt et al., 2014). Similarly, the L-arginine production could be the target of further metabolic engineering, *e.g.*, by deletion of *farR*, by increasing the NADPH-level and via overexpression of L-arginine biosynthesis genes, especially of the production rate-controlling step encoded by *argGH* (Park et al., 2014). In addition to amino acid biosynthesis, other parameters such as D-glucose uptake, amino acid uptake and amino acid secretion may also be considered. The observed "dilution effect" could indicate a CoNoS limitation due to an insufficient secretion rate of the cross-fed amino acid, as well as difficulties of the strains to take up the corresponding amino acid when present only in low concentrations.

Specifically, L-arginine was shown to be exported via LysE and CgmA (Lubitz et al., 2016), while for L-leucine, BrnFE was identified as an exporter (Kennerknecht et al., 2002). Therefore, overexpression of these export systems could be a valuable option to increase amino acid secretion and thus optimize crossfeeding in the ΔARG ↔ ΔLEU CoNoS. Interestingly, there is currently no known import mechanism for L-arginine in *C. glutamicum*. This might be due to the fact that this amino acid is not metabolizable or even harmful for the cells as shown recently for a corresponding dipeptide supplementation experiment (Lubitz et al., 2016). However, with the L-arginine auxotrophic strain ΔARG growing similar to the WT (Fig. 3A), some L-arginine import must exist. On the other hand, the amino acid import of L-leucine could likely be improved by overexpression of the branched-chain amino acid importer BrnQ (Tauch et al., 1998). Since the K_m value was determined to be 9 μM and the uptake followed conventional Michaelis-Menten kinetics (Ebbighausen et al., 1989), the initial low amino acid concentrations in liquid culture could be considered as the main problem of the CoNoS to overcome.

This factor fits well with an example of a co-culture of two amino acid auxotrophic *E. coli* strains: Evolution of this community in an unstructured environment led to increased formation of spatial structures of multicellular aggregates to enhance metabolite exchange (Preussger et al., 2020). The use of adaptive laboratory evolution (ALE) could indeed be a viable approach to address the bottlenecks in CoNoS development, and the general feasibility of the repetitive batch approach has been successfully demonstrated (see Fig. 6C). Because many targets for optimization, *e.g.*, the mechanism of L-arginine import, are unknown, the ALE approach is particularly useful for identifying novel uptake and production traits (Radek et al., 2017; Tenhaef et al., 2018). Identification and characterization of these traits would provide valuable insights not only into synthetic co-cultures but also into the platform organism *C. glutamicum* in general.

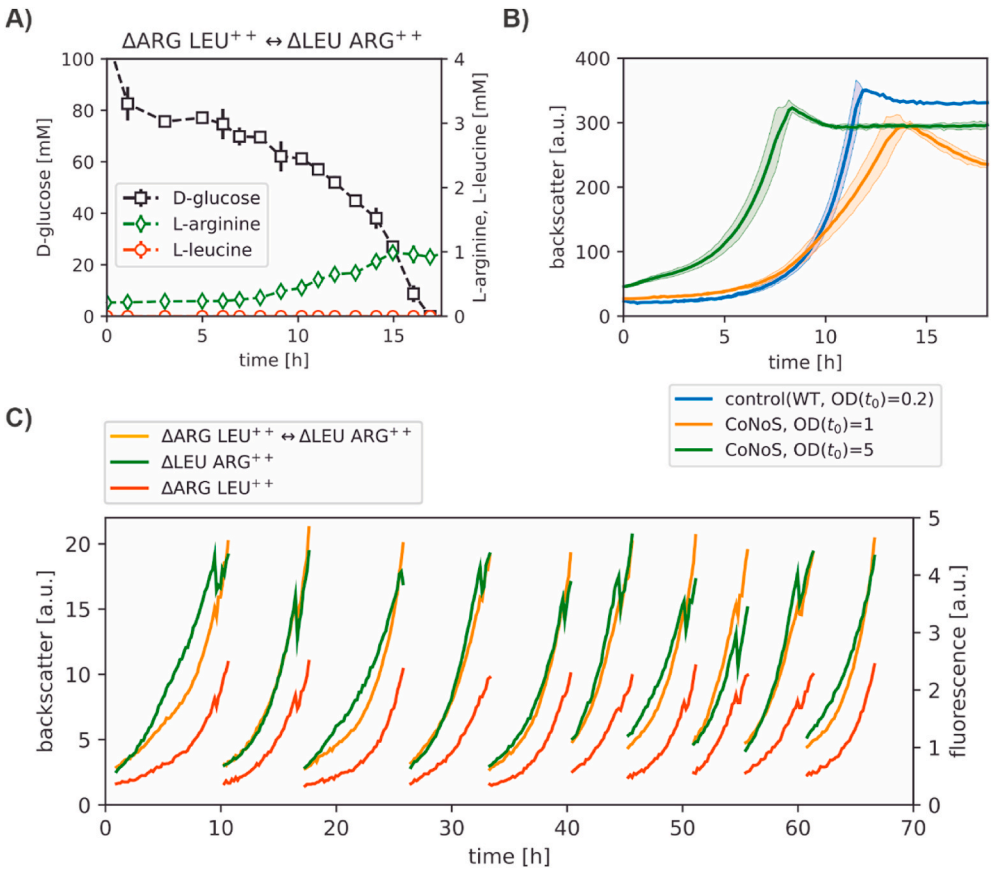

Fig. 6. Detailed phenotyping of improved ΔARG LEU^{++} ↔ ΔLEU ARG^{++} CoNoS and final stability test. A) Transient sampling experiment with the co-culture grown in triplicate in CGXII medium. B) Effect of inoculation density on growth performance. C) Repetetive batch cultivation with online monitoring of total biomass (orange) and fractions of CoNoS partners ΔARG LEU^{++} (red) and ΔLEU ARG^{++} (green), respectively. The fully automated experiment was performed on a Mini Pilot Plant and each batch was started with freshly stored CGXII medium inoculated with 12% v v^{-1} of the previous batch after the predefined backscatter of BS = 15 was reached (for technical details see (Radek et al., 2017)). To investigate a potential effect of the inoculum density, the last 5 batched where inoculated with 24% v v^{-1} of the previous batch.

4. Conclusions

In the present work, following a model-based design, several amino acid-auxotrophic *C. glutamicum* strains were constructed by deleting the entire biosynthetic machinery for the target amino acid. In most cases, the fitness of the newly constructed strains was comparable to that of the control strain when cultured in amino acid-supplemented media, confirming the suitability of the strain in a CoNoS. Releasing feedback inhibition by metabolic engineering proved to be a successful strategy to enhance amino acid exchange and improve the growth performance of new and further engineered CoNoS. The best performing CoNoS ΔARG LEU^{++} ↔ ΔLEU ARG^{++} exhibited a specific growth rate of 83% and a biomass titer of 86% of the control strain, making it the fastest co-culture of two auxotrophic *C. glutamicum* strains to date.

To conclude, synthetic communities can be established using genome-reduced microorganisms that grow with mutual dependency. We have achieved the goal of establishing CoNoS for efficient delivery of biocatalysts for amino acid production. To use CoNoS for production, one needs to take a further step by developing a co-culture/process design that allows enrichment of one of the producer strains and efficiently blocks unwanted consumption of the target amino acid. Here, the implementation of synthetic regulatory growth switches in combination with “edible” inducers is conceivable. This would allow growth of CoNoS to sufficient cell density, enrichment of the targeted production strain, and continuation of the process for efficient amino acid production.

Finally, the presented approach is general and should be applicable to any target product that ensures the necessary interdependence of CoNoS partners for the co-culture to reach sufficient density prior switching to production. In this regard, designs with couplings through native byproducts are also conceivable, which could be particularly interesting for the production of more complex molecules in heterologous pathways.

5. Materials and methods

5.1. Model-based design of CoNoS

For the model-based design and analysis of CoNoS, two different-sized models of the *C. glutamicum* metabolic network were created, namely a genome-scale model (GSM) and a focused model of the central metabolism, respectively. The GSM was derived from the published model iEZ475 (Zelle et al., 2015) and has some minor modifications, which are discussed below. The focused model was created from the GSM by defining the system boundaries around the amino acid biosynthetic pathways and omitting all reactions outside the central metabolism, such as cell wall synthesis. This resulted in a simplified model with 56% fewer reactions and 51% fewer metabolites. In both cases, the transport of amino acids was modeled by assuming free diffusion, and the transport reactions for ARG, GLN, PRO, SER, and TRP that were missing in the original GSM were additionally introduced.

The COnstraint-Based Reconstruction and Analysis (COBRA) toolbox (Heirendt et al., 2019) under MATLAB (Mathworks, R2017b) was applied for cFBA of single amino acid auxotrophic *C. glutamicum* strains. According to the experimental conditions, D-glucose was defined as the sole carbon and energy source, and for quantitative growth rate predictions, the PTS-coupled uptake rate was constrained to the measured rate of 5.6 mmol g_{CDW} h^{-1}. Biomass growth was defined as optimization criteria. Amino acid auxotrophies were mimicked by constraining single essential reactions of the respective amino acid biosynthesis pathway to carry zero flux.

Simulation of different co-cultures based on the CoNoS approach and prediction of the abundance of the underlying auxotrophic strains was performed using the expansion of single-species cFBA (Chan et al.,

2017). In short, SteadyCom seeks to predict the maximum community growth rate of two or more microbial species at community steady-state conditions. The resulting extended linear program is then solved by stepwise optimization of the community growth rate. For the CoNoS simulation, the subnetworks were connected by defining exchange reactions for the corresponding essential amino acids.

5.2. Strain construction

All *C. glutamicum* strains used in this study are listed in Table 1 and are based either on the wild type *C. glutamicum* ATCC 13032 or on its genome reduced variant C1* (Baumgart et al., 2018). For molecular cloning, *Escherichia coli* DH5α (Hanahan, 1983) was used as host. The plasmids used are listed in Table S1 and the oligonucleotides in Table S2. For the construction of deletion strains and for integrating mutations in *C. glutamicum*, the pK19*mobsacB*-system was applied, operating by introducing double crossover events as described previously (Keilhauer et al., 1993; Schafer et al., 1994). The genes deleted for constructing the auxotrophic strains are represented in Fig. 2C. The primer used for the Colony-PCRs to check for mutations or deletions as well as for differentiating between the different auxotrophic strains in the CoNoS are listed in Table S3.

5.3. Bacterial strains and growth conditions

For cultivation of *E. coli* strains, lysogeny broth (LB) agar plates or liquid LB (Bertani, 1951) were used at 37 °C. For strains with plasmids, 50 μg mL^{-1} kanamycin was added. For *C. glutamicum*, either brain heart infusion (BHI) medium (Difco Laboratories, Detroit, USA) or defined CGXII medium (Keilhauer et al., 1993) was used at 30 °C. All cultivations except those for strain construction performed in this study were carried out in biological triplicates. The cultivations were performed in defined CGXII medium consisting of (per litre) 20 g of $(NH_4)_2SO_4$, 5 g of urea, 1 g of KH_2PO_4, 1 g of K_2HPO_4, 0.25 g of $MgSO_4 \cdot 7\ H_2O$, 42 g of 3-morpholinopropanesulfonic acid, 13.25 mg of $CaCl_2$, 10 mg of $FeSO_4 \cdot 7\ H_2O$, 10 mg of $MnSO_4 \cdot H_2O$, 1 mg of $ZnSO_4 \cdot 7\ H_2O$, 0.313 mg of $CuSO_4$, 0.02 mg of $NiCl_2 \cdot 6\ H_2O$, 0.2 mg of biotin (pH 7), 20 g of D-glucose, and 0.03 g of protocatechuic acid (PCA). During medium preparation, some substances were added sterile after autoclaving (D-glucose, PCA, biotin, $MgSO_4 \cdot 7\ H_2O$, $CaCl_2$, $FeSO_4 \cdot 7\ H_2O$, $MnSO_4 \cdot H_2O$, $ZnSO_4 \cdot 7\ H_2O$, $CuSO_4$, $NiCl_2 \cdot 6\ H_2O$) and pH 7.0 was adjusted with 8 M NaOH. In experiments with supplemented CGXII medium, amino acids supplement was added sterile according to the strain requirements. In each mono and co-culture showed in this study, each strain was pre-cultivated in a mono-culture in supplemented CGXII medium inoculated with a single colony from the correspondent strain. After two days of incubation at 30 °C, 250 rpm, the pre-cultures were centrifuged, the pellet was re-suspended in sterile 0.9% (w v^{-1}) NaCl, and used to inoculate the main cultures.

5.4. Microscale cultivations and transient sampling

The main cultures were performed in 48-well FlowerPlates (m2p-labs GmbH, Germany) with dissolved oxygen and pH optodes in a BioLector (m2p-labs GmbH, Germany) at 1400 rpm, 85% humidity and 30 °C. Inoculated FlowerPlates were covered with a sterile gas permeable foil (m2p-labs GmbH, Baesweiler). Mono-cultures were started at an optical density of $OD_{600} \approx 0.2$ and co-cultures were started at an overall optical density of $OD_{600} \approx 1$ by inoculating the correspondent pre-cultures, unless differently specified. The higher CoNoS inoculum density allow an initial medium enrichment with the shared amino acid.

For characterizing the substrate uptake and amino acid production rates of the analyzed strains, automated harvesting of cultures was performed using a Freedom Evo 200 (Tecan, Switzerland) robotic platform which embeds a BioLector cultivation device. The robotic workstation employs a liquid handling arm using eight steel needles, a gripper arm for transport of plates, a Rotanta 460 RSC MTP centrifuge (Hettich) and an Infinite M 200 Pro MTP reader (Tecan). For cultures, 15 ml of supplemented CGXII medium was inoculated with pre-cultivated cells in triplicates as described before. An aliquot of the inoculated media was centrifuged (4500 rpm for 10 min) and the supernatant was stored for HPLC analysis and glucose assays. For each replicate, 800 μL of the inoculated media were distributed in 16 wells of a 48-well FlowerPlate. Inoculated FlowerPlates were covered with a sterile gas permeable foil and the main culture was carried out at 1400 rpm, 85% humidity and 30 °C. For each replicate, one well was harvested and centrifuged (4500 rpm for 10 min) every hour since the beginning of the cultivation using the automated platform. Each supernatant was stored chilled and further processed using the robotic platform in a separated workflow.

At the end of the first automated workflow, the stored cell-free supernatants were filtered through a 96 well filterplate (AcroPrep™ Advance, 1 ml, 0.2 μm Supor® membrane, PES) using the centrifuge and were appropriately diluted with MilliQ water preparing 4 different 96-well micro titer plates (MTP), two MTP were used for amino acid quantification and two for glucose quantification.

5.5. Supernatant analysis

D-glucose quantification was performed with a hexokinase assay (DiaSys) in MTP containing the properly diluted cell-free supernatant. Using the robotic platform described before, 20 μL of diluted cell-free supernatants were mixed with 280 μL assay mastermix and incubated for 6 min at room temperature before absorption measurement at 365 nm in the MTP reader. Results were calibrated against D-glucose serial dilution standards processed in the same way.

For amino acid quantification, 50 mM α-Aminobutyric acid (AABA) was added as an internal standard to MTPs containing the properly diluted cell-free supernatant. Separation of amino acids was performed on a HPLC system (Agilent 1100 Infinity, AgilentTechnologies, Santa Clara, CA). The method used involves a pre-column (Phenomenex, KrudeKatcher Ultra HPLC In-line Filter 0.5 μm Depth Filter x 0.004 in ID) and a reverse phase column (Kinetex 5 μm EVO C18 100 °A, 150 × 4.6 mm) as stationary phase, buffer A (26 mM $NaH_2PO_4 \cdot 2H_2O$, 14.8 mM $Na_2HPO_4 \cdot 2H_2O$, 7.2 pH) + 0.5% tetrahydrofuran and buffer B (50% buffer A, 35% methanol, 15% acetonitrile) with a flow rate of 0.9 mL min^{-1} as mobile phase, a column temperature of 40 °C and an injection volume of 15 μL. Amino acids were separated with the following linear gradient elution conditions (min/B%): 0/20, 7/80, 14/80, 17/100, 23/100, 24/20 and 30/20. Pre-column derivatization with Phthaldialdehyde (OPA) reagent (Sigma-Aldrich, ready-to-use mix) was performed in an automated procedure where 5 μL of OPA, 5 μL of sample and 5 μL of water were mixed in the injection loop 6 times and incubated for 1 min. Detection of amino acids was performed using a fluorescence detector (Agilent 1100 FLD) with excitation wavelength of 230 nm and emission wavelength of 460 nm. Quantification of target amino acids was performed relatively to the internal standard measured in each sample in order to correct variation of signal due to different derivatization conditions within the sample.

5.6. Determination of specific rates

Specific growth rates were determined by processing the raw backscatter data from BioLector experiments using the bletl tool and following the spline-based approximation approach (Osthege et al., 2022). Data visualization was performed using matplotlib (Hunter, 2007).

Specific rates for amino acid uptake and secretion of the ΔLEU ARG^{+}, ΔLEU ARG^{++} and the ΔARG LEU^{++} strain were determined by process modelling. Based on the two monoculture (with three replicates, cf. Fig. 4B) and the final co-culture (with two replicates, cf. Fig. 5A) experiments, three partially dependent models were formulated to

describe the growth and production kinetics of the strains involved. The models are structured by one extracellular compartment for the liquid phase and one intracellular compartment covering either one (i.e. monoculture), or two (i.e. co-culture) engineered strains (cf. Fig. 5B). For model implementation, validation and analysis we used the open-source, python-based modeling tool pyFOOMB (Hemmerich et al., 2020). For all three models the corresponding Jupyter notebooks are provided in GitHub (https://github.com/JuBiotech/Supplement-to-Schito-et-al.-CoNoS-MetabEng-2022) and contain detailed descriptions of all modeling procedures and fitting results.

5.7. Microfluidics

The microfluidic chip fabrication is based on a soft lithography protocol described previously (Grünberger et al., 2013). The PDMS-based microfluidic cultivation device (Kaganovitch et al., 2018) consists of 6 cultivation rows each with several cultivation chambers, each 60 μm × 100 μm x 1 μm (width, length, height) in size. The chamber height enforces the cells to grow in monolayers. Each cultivation chamber is coupled to a medium reservoir resulting in a total cultivation volume of 606 pL in total. The cultivation chamber and the medium reservoir are separated by a thin PDMS double grid structure, which prevent cells from entering the medium reservoir and at the same time ensures diffusive medium exchange between the cultivation chamber and the reservoir. To prevent the evaporation of the low cultivation volumes, the following measures were implemented: an additional water-filled top layer and additional side channels around the cultivation chambers were used and perfused with water during the cultivation. Before inoculating the microfluidic cultivation device the cells were pre-cultivated in mono culture with CGXII medium supplemented with the required amino acid amount as described previously (see Bacterial strains and growth conditions). Cell-free supernatant was resuspended in 0.9% w v^{-1} NaCl and mixed in a ratio 1:1 with the partner strain for establishing a CoNoS. The CoNoS cell suspension was diluted to an OD_{600} of 0.5 and flushed through the medium channels by gently applying pressure to a 1 mL syringe. This flow randomly inoculated single cells of both strains into several chambers. Afterwards fresh media was flushed through the medium channels for 15 min at 200 nl min (nemeSYS syringe pumps, Cetoni GmbH, Germany). By applying pressurized air (600 mbar) at the channel inlet, the residual medium is expelled out of the medium channel, resulting in individual isolated cultivation chambers. Before starting the experiments, the water reservoir and the side channels were filled with deionized water under low pressure (p_{water} reservoir = 40 mbar, p_{side} channel = 90 mbar). To monitor the cultivation a time-lapse microscope setup was used that consists of an inverted fluorescence microscope (Ti Eclipse, Nikon) equipped with a 100× oil immersion objective (Plan Apochromat λ Oil, N.A. 1.45 and a working distance of 170 μm, Nikon Microscopy). Stable temperature conditions were ensured by operating the microscope in an incubation chamber (TempController, 2000-2, PECON, Germany). All cultivations were performed at 30 °C. For time-lapse imaging, phase contrast and fluorescence images were acquired with 100 ms exposure, taking an image every 30 min for the wild type strains and every 20 min for the co-cultures. For *C. glutamicum* WT cultivations, a CMOS camera ANDOR Neo/Zyla (ANDOR, Oxford Instruments, England) was used in combination with the Intensilight (Nikon Microscopy) light source. For the *C. glutamicum* ΔARG LEU^{++}::P_{tac}-crimson ↔ ΔLEU ARG^{++}::P_{tac}-eYFP CoNoS cultivations, a DS-Qi2 camera (Nikon Microscopy) in combination with the sola light engine (Lumencor, USA) was used. For fluorescence measurements, NIKON excitation and fluorescence filter cubes for eYFP (FITC, excitation: 465–495 nm, dichroic mirror: 505 nm, emission: 515–555 nm) and for crimson(excitation: 540–580 nm, dichroic mirror: 593 nm, emission: 600–684 nm) (AHF Analysetechnik, Germany) were used. Acquired time-lapse series were manually pre-processed. This included image alignment, brightness adjustments and cropping the region of interest using the software Fiji (Schindelin et al., 2012).

5.8. Image and data analysis

Time-lapse videos were segmented using Omnipose, a deep neural network approach pre-trained on a comprehensive set of bacterial systems (Cutler et al., 2021), and individual cell contours were computed for every frame. Artifacts were removed by constraining the minimal (0.5 μm^2) and maximally (4.5 μm^2) allowed cell area and enforcing a maximal length-width ratio (5.5) per cell. The resulting cell contours were used to compute the median red and green fluorescent colors inside the cell body using Gaussian filtered fluorescence images. The extracted colors were normalized per frame, and cells below a fluorescence signal of 35% were discarded. Depending on the dominant fluorescence channel, remaining cells were assigned "green" or "red" labels yielding cell counts and ratio. The results were then manually checked. Due to the large number of cells in the time-lapse (>100k), the contour computation and fluorescence extraction were parallelized to reduce the total computation time to less than 21 min on an AMD Ryzen 7 1800X and an NVIDIA GeForce RTX 2060 GPU. The code and visualizations for the analysis are available in GitHub (https://github.com/JuBiotech/Supplement-to-Schito-et-al.-CoNoS-MetabEng-2022).

Author contributions

Simone Schito: Methodology, Validation, Investigation, Writing - Original Draft, Visualization.

Rico Zuchowski: Methodology, Validation, Investigation, Writing - Original Draft.

Daniel Bergen: Methodology, Formal analysis, Visualization.

Daniel Strohmeier: Methodology, Formal analysis, Data Curation.

Bastian Wollenhaupt: Methodology, Data Curation.

Philipp Menke: Investigation.

Johannes Seiffarth: Software, Formal analysis, Visualization.

Katharina Nöh: Data Curation, Writing - Review & Editing, Supervision.

Dietrich Kohlheyer: Writing - Review & Editing, Supervision, Funding acquisition.

Michael Bott: Resources, Writing - Review & Editing.

Wolfgang Wiechert: Resources, Writing - Review & Editing.

Meike Baumgart: Conceptualization, Methodology, Writing - Review & Editing, Supervision, Funding acquisition.

Stephan Noack: Conceptualization, Methodology, Writing - Review & Editing, Visualization, Supervision, Project administration, Funding acquisition.

Declaration of competing interest

The authors declare that they have no conflict of interest.

Acknowledgements

We thank Niklas Tenhaef and Michael Osthege for programming support on the Mini Pilot Plant. We thank Eric von Lieres and Martin Beyβ for providing computational infrastructure and technical support throughout the project. Christina Mack helped constructing auxotrophic strains. We gratefully acknowledge support and funding from the Deutsche Forschungsgemeinschaft (priority program SPP2170, project no. 427904493 and 428038451). Open Access publication funded by the Deutsche Forschungsgemeinschaft (DFG, German Research Foundation) – 491111487.

Appendix A. Supplementary data

Supplementary data to this article can be found online at https://doi.org/10.1016/j.ymben.2022.06.004.

References

Alifano, P., Fani, R., Liò, P., Lazcano, A., Bazzicalupo, M., Carlomagno, M.S., Bruni, C.B., 1996. Histidine biosynthetic pathway and genes: structure, regulation, and evolution. Microbiol. Rev. 60, 44–69.

Barona-Gómez, F., Hodgson, D.A., 2003. Occurrence of a putative ancient-like isomerase involved in histidine and tryptophan biosynthesis. EMBO Rep. 4, 296–300.

Baumgart, M., Unthan, S., Rückert, C., Sivalingam, J., Grünberger, A., Kalinowski, J., Bott, M., Noack, S., Frunzke, J., 2013. Construction of a prophage-free variant of *Corynebacterium glutamicum* ATCC 13032 for use as a platform strain for basic Research and industrial biotechnology. Appl. Environ. Microbiol. 79, 6006–6015.

Baumgart, M., Unthan, S., Kloß, R., Radek, A., Polen, T., Tenhaef, N., Müller, M.F., Küberl, A., Siebert, D., Brühl, N., Marin, K., Hans, S., Krämer, R., Bott, M., Kalinowski, J., Wiechert, W., Seibold, G., Frunzke, J., Rückert, C., Wendisch, V.F., Noack, S., 2018. *Corynebacterium glutamicum* chassis C1*: building and testing a novel platform host for synthetic biology and industrial biotechnology. ACS Synth. Biol. 7, 132–144.

Bertani, G., 1951. Studies on lysogenesis. I. The mode of phage liberation by lysogenic *Escherichia coli*. J. Bacteriol. 62, 293–300.

Chan, S.H.J., Simons, M.N., Maranas, C.D., 2017. SteadyCom: predicting microbial abundances while ensuring community stability. PLoS Comput. Biol. 13, e1005539.

Cutler, K.J., Stringer, C., Wiggins, P.A., Mougous, J.D., 2021. Omnipose: a High-Precision Morphology-independent Solution for Bacterial Cell Segmentation. bioRxiv.

D'Souza, G., Waschina, S., Pande, S., Bohl, K., Kaleta, C., Kost, C., 2014. Less IS more: selective advantages can explain the prevalent loss of biosynthetic genes in bacteria. Evolution 68, 2559–2570.

Ebbighausen, H., Weil, B., Krämer, R., 1989. Transport of branched-chain amino acids in *Corynebacterium glutamicum*. Arch. Microbiol. 151, 238–244.

Eggeling, L., Bott, M., 2005. Handbook of *Corynebacterium glutamicum*. CRC Press, Boca Raton.

Grünberger, A., Probst, C., Heyer, A., Wiechert, W., Frunzke, J., Kohlheyer, D., 2013. Microfluidic picoliter bioreactor for microbial single-cell analysis: fabrication, system setup, and operation. JoVE 82, e50560.

Hanahan, D., 1983. Studies on transformation of *Escherichia coli* with plasmids. J. Mol. Biol. 166, 557–580.

Heery, D.M., Fitzpatrick, R., Dunican, L.K., 1994. A sequence from a tryptophan-hyperproducing strain of *Corynebacterium glutamicum* encoding resistance to 5-methyltryptophan. Biochem. Biophys. Res. Commun. 201, 1255–1262.

Heirendt, L., Arreckx, S., Pfau, T., Mendoza, S.N., Richelle, A., Heinken, A., Haraldsdóttir, H.S., Wachowiak, J., Keating, S.M., Vlasov, V., 2019. Creation and analysis of biochemical constraint-based models using the COBRA Toolbox v. 3.0. Nat. Protoc. 14, 639–702.

Hemmerich, J., Tenhaef, N., Wiechert, W., Noack, S., 2020. pyFOOMB: Python framework for object oriented modeling of bioprocesses. Eng. Life Sci. 21, 242–257.

Hunter, J.D., 2007. Matplotlib: a 2D graphics environment. Comput. Sci. Eng. 9, 90–95.

Ikeda, M., Mitsuhashi, S., Tanaka, K., Hayashi, M., 2009. Reengineering of a *Corynebacterium glutamicum* L-arginine and L-citrulline producer. Appl. Environ. Microbiol. 75, 1635–1641.

Kaganovitch, E., Steurer, X., Dogan, D., Probst, C., Wiechert, W., Kohlheyer, D., 2018. Microbial single-cell analysis in picoliter-sized batch cultivation chambers. N. Biotech. 47, 50–59.

Kalinowski, J., Bathe, B., Bartels, D., Bischoff, N., Bott, M., Burkovski, A., Dusch, N., Eggeling, L., Eikmanns, B.J., Gaigalat, L., Goesmann, A., Hartmann, M., Huthmacher, K., Krämer, R., Linke, B., McHardy, A.C., Meyer, F., Möckel, B., Pfefferle, W., Pühler, A., Rey, D.A., Rückert, C., Rupp, O., Sahm, H., Wendisch, V.F., Wiegräbe, I., Tauch, A., 2003. The complete *Corynebacterium glutamicum* ATCC 13032 genome sequence and its impact on the production of L-aspartate-derived amino acids and vitamins. J. Biotechnol. 104, 5–25.

Keilhauer, C., Eggeling, L., Sahm, H., 1993. Isoleucine synthesis in *Corynebacterium glutamicum*: molecular analysis of the *ilvB-ilvN-ilvC* operon. J. Bacteriol. 175, 5595–5603.

Kennerknecht, N., Sahm, H., Yen, M.-R., Pátek, M., Saier, M.H., Eggeling, L., 2002. Export of L-isoleucine from *Corynebacterium glutamicum*: a two-gene-encoded member of a new translocator family. J. Bacteriol. 184, 3947–3956.

Kinoshita, S., Udaka, S., Shimono, M., 1957. Studies on the amino acid fermentation. Part I. Production of L-glutamic acid by various microorganisms. J. Gen. Appl. Microbiol. 3, 193–205.

Kulis-Horn, R.K., Persicke, M., Kalinowski, J., 2014. Histidine biosynthesis, its regulation and biotechnological application in *Corynebacterium glutamicum*. Microb. Biotechnol. 7, 5–25.

Kulis-Horn, R.K., Persicke, M., Kalinowski, J., 2015. *Corynebacterium glutamicum* ATP-phosphoribosyl transferases suitable for L-histidine production–Strategies for the elimination of feedback inhibition. J. Biotechnol. 206, 26–37.

Lubitz, D., Jorge, J.M., Pérez-García, F., Taniguchi, H., Wendisch, V.F., 2016. Roles of export genes *cgmA* and *lysE* for the production of L-arginine and L-citrulline by *Corynebacterium glutamicum*. Appl. Microbiol. Biotechnol. 100, 8465–8474.

Matsui, K., Miwa, K., Sano, K., 1987. Two single-base-pair substitutions causing desensitization to tryptophan feedback inhibition of anthranilate synthase and enhanced expression of tryptophan genes of *Brevibacterium lactofermentum*. J. Bacteriol. 169, 5330–5332.

McCarty, N.S., Ledesma-Amaro, R., 2019. Synthetic biology tools to engineer microbial communities for biotechnology. Trends Biotechnol. 37, 181–197.

Mormann, S., Lömker, A., Rückert, C., Gaigalat, L., Tauch, A., Pühler, A., Kalinowski, J., 2006. Random mutagenesis in *Corynebacterium glutamicum* ATCC 13032 using an IS6100-based transposon vector identified the last unknown gene in the histidine biosynthesis pathway. BMC Genom. 7, 205.

Mundhada, H., Schneider, K., Christensen, H.B., Nielsen, A.T., 2016. Engineering of high yield production of L-serine in *Escherichia coli*. Biotechnol. Bioeng. 113, 807–816.

Noack, S., Baumgart, M., 2019. Communities of niche-optimized strains: small-genome organism consortia in bioproduction. Trends Biotechnol. 37, 126–139.

Noack, S., Voges, R., Gätgens, J., Wiechert, W., 2017. The linkage between nutrient supply, intracellular enzyme abundances and bacterial growth: new evidences from the central carbon metabolism of *Corynebacterium glutamicum*. J. Biotechnol. 258, 13–24.

Osthege, M., Tenhaef, N., Zyla, R., Müller, C., Hemmerich, J., Wiechert, W., Noack, S., Oldiges, M., 2022. bletl-A Python package for integrating BioLector microcultivation devices in the Design-Build-Test-Learn cycle. Eng. Life Sci. 22, 242–259.

O'Brien, E.J., Utrilla, J., Palsson, B.O., 2016. Quantification and classification of *E. coli* proteome utilization and unused protein costs across environments. PLoS Comput. Biol. 12, e1004998.

Paczia, N., Nilgen, A., Lehmann, T., Gätgens, J., Wiechert, W., Noack, S., 2012. Extensive exometabolome analysis reveals extended overflow metabolism in various microorganisms. Microb. Cell Factories 11, 122.

Pande, S., Merker, H., Bohl, K., Reichelt, M., Schuster, S., de Figueiredo, L.F., Kaleta, C., Kost, C., 2014. Fitness and stability of obligate cross-feeding interactions that emerge upon gene loss in bacteria. ISME J. 8, 953–962.

Park, S.H., Kim, H.U., Kim, T.Y., Park, J.S., Kim, S.-S., Lee, S.Y., 2014. Metabolic engineering of *Corynebacterium glutamicum* for L-arginine production. Nat. Commun. 5, 4618.

Peters-Wendisch, P., Stolz, M., Etterich, H., Kennerknecht, N., Sahm, H., Eggeling, L., 2005. Metabolic engineering of *Corynebacterium glutamicum* for L-serine production. Appl. Environ. Microbiol. 71, 7139–7144.

Preussger, D., Giri, S., Muhsal, L.K., Oña, L., Kost, C., 2020. Reciprocal fitness feedbacks promote the evolution of mutualistic cooperation. Curr. Biol. 30, 3580–3590 e7.

Radek, A., Tenhaef, N., Müller, M.F., Brüsseler, C., Wiechert, W., Marienhagen, J., Polen, T., Noack, S., 2017. Miniaturized and automated adaptive laboratory evolution: evolving *Corynebacterium glutamicum* towards an improved D-xylose utilization. Bioresour. Technol. 245, 1377–1385.

San Roman, M., Wagner, A., 2018. An enormous potential for niche construction through bacterial cross-feeding in a homogeneous environment. PLoS Comput. Biol. 14, e1006340.

Schafer, A., Tauch, A., Jager, W., Kalinowski, J., Thierbach, G., Puhler, A., 1994. Small mobilizable multi-purpose cloning vectors derived from the *Escherichia coli* plasmids pK18 and pK19: selection of defined deletions in the chromosome of *Corynebacterium glutamicum*. Gene 145, 69–73.

Schindelin, J., Arganda-Carreras, I., Frise, E., Kaynig, V., Longair, M., Pietzsch, T., Preibisch, S., Rueden, C., Saalfeld, S., Schmid, B., Tinevez, J.Y., White, D.J., Hartenstein, V., Eliceiri, K., Tomancak, P., Cardona, A., 2012. Fiji: an open-source platform for biological-image analysis. Nat. Methods 9, 676–682.

Shou, W., Ram, S., Vilar, J.M.G., 2007. Synthetic cooperation in engineered yeast populations. Proc. Natl. Acad. Sci. 104, 1877.

Tauch, A., Hermann, T., Burkovski, A., Krämer, R., Pühler, A., Kalinowski, J., 1998. Isoleucine uptake in *Corynebacterium glutamicum* ATCC 13032 is directed by the *brnQ* gene product. Arch. Microbiol. 169, 303–312.

Tenhaef, N., Brüsseler, C., Radek, A., Hilmes, R., Unrean, P., Marienhagen, J., Noack, S., 1957. Production of D-xylonic acid using a non-recombinant Corynebacterium glutamicum strain. Bioresour. Technol. 268, 332–339.

Unthan, S., Baumgart, M., Radek, A., Herbst, M., Siebert, D., Brühl, N., Bartsch, A., Bott, M., Wiechert, W., Marin, K., Hans, S., Krämer, R., Seibold, G., Frunzke, J., Kalinowski, J., Rückert, C., Wendisch, V.F., Noack, S., 2015. Chassis organism from *Corynebacterium glutamicum*–a top-down approach to identify and delete irrelevant gene clusters. Biotechnol. J. 10, 290–301.

Vidal, L., Pinsach, J., Striedner, G., Caminal, G., Ferrer, P., 2008. Development of an antibiotic-free plasmid selection system based on glycine auxotrophy for recombinant protein overproduction in *Escherichia coli*. J. Biotechnol. 134, 127–136.

Voges, R., Corsten, S., Wiechert, W., Noack, S., 2015. Absolute quantification of *Corynebacterium glutamicum* glycolytic and anaplerotic enzymes by QconCAT. J. Proteomics 113, 366–377.

Vogt, M., Haas, S., Klaffl, S., Polen, T., Eggeling, L., van Ooyen, J., Bott, M., 2014. Pushing product formation to its limit: metabolic engineering of *Corynebacterium glutamicum* for L-leucine overproduction. Metab. Eng. 22, 40–52.

Wehrmann, A., Morakkabati, S., Krämer, R., Sahm, H., Eggeling, L., 1995. Functional analysis of sequences adjacent to *dapE* of *Corynebacterium glutamicum* reveals the presence of *aroP*, which encodes the aromatic amino acid transporter. J. Bacteriol. 177, 5991–5993.

Wynands, B., Otto, M., Runge, N., Preckel, S., Polen, T., Blank, L.M., Wierckx, N., 2019. Streamlined *Pseudomonas taiwanensis* VLB120 chassis strains with improved bioprocess features. ACS Synth. Biol. 8, 2036–2050.

Yang, D.-D., Alexander, A., Kinnersley, M., Cook, E., Caudy, A., Rosebrock, A., Rosenzweig, F., Cann, I., 2020. Fitness and productivity increase with ecotypic diversity among *Escherichia coli* strains that coevolved in a simple, constant environment. Appl. Environ. Microbiol. 86 e00051-20.

Zelle, E., Nöh, K., Wiechert, W., 2015. Growth and production capabilities of *Corynebacterium glutamicum*: interrogating a genome-scale metabolic network model. In: *Corynebacterium glutamicum*: from Systems Biology to Biotechnological Applications. Caister Academic Press, pp. 39–54.